Soft Matter

RSC Publishing

PAPER

Suppressed surface dynamics of poly(methyl methacrylate) chains in the corona of collapsed dry micelles tethered by a fluorinated block core†

Cite this: *Soft Matter*, 2013, **9**, 5428

Biao Zuo, Wanglong Liu, Hao Fan, Yizhi Zhang, Tingting He and Xinping Wang*

The effect of chain constraint on the surface dynamic of poly(methyl methacrylate) (PMMA) was investigated in the context of polymer tethering to a micelle core. Film surfaces dominated by either poly(methyl methacrylate) (PMMA) tethered by a poly(2-perfluorooctylethyl methacrylate) (PFMA) micelle core or non-micellized free PMMA chains are fabricated by spin coating a solution of PMMA end-capped with various numbers of FMA units onto silica substrates. By measuring the surface rearrangement kinetics of these films under thermal annealing, the onset temperature of rearrangement (T_R^{onset}) and the activation barrier for relaxation (E_a) of surface PMMA chains are determined. It is found that the T_R^{onset} and E_a of the PMMA micellized chains are 83 °C and 317 kJ mol^{-1}, respectively, which are higher than those of the non-micellized PMMA free chains (70 °C and 164 kJ mol^{-1}). The T_R^{onset} and E_a of PMMA in the corona increase linearly with increasing compactness of the PFMA core. The higher T_R^{onset} and E_a values demonstrate the reduced mobility of surface PMMA segments tethered to a micelle core. The constraint of conformational freedom, reduction of free volume and increment of chain packing density are proposed as the speculative origins for this depressed dynamic of poly(methyl methacrylate) chains in the corona of collapsed dry micelles tethered by fluorinated block core.

Received 22nd January 2013
Accepted 20th March 2013

DOI: 10.1039/c3sm50237f

www.rsc.org/softmatter

1 Introduction

The dynamics of polymer chains at the air–polymer interface is of significance for the many practical applications of materials, such as permselective membranes, biomaterials, adhesives and lubricants.[1,2] Many recent technological devices have been reduced to the nanometer scale, so that the performance of thin film coatings and nano-devices are intimately correlated with the dynamic properties of the chains residing on a surface.[3–6] For the past two decades, the investigations of chain dynamics on polymer surfaces have attracted great attention[6–11] and there are considerable data for systems such as atactic polystyrene (PS)[6–9] and poly(methyl methacrylate) (PMMA)[10,12–15] in particular. The target polymeric films for research were usually prepared by spin coating, and subjected to thermal annealing at a temperature above the corresponding glass transition temperature (T_g) to recover the equilibrium "melt-like" structure. In these situations, the polymer chains were homogeneously distributed on the surface without any chain ordered structure at long-range or preferred interaction. The results showed that the quasi-equilibrated chains on free surfaces exhibited faster relaxation and lower T_g compared with the molecules in bulk,[7–11] which are very representative of the general behavior for macromolecular motions on a surface.

However, in some cases the surface chain conformations deviate from those of equilibrium state films and the surface chains may exhibit various aggregative structures, which may result in a deviation of the chain dynamics from those of the equilibrated "melt-like" surface chains.[15–20] Some reports have shown that the molecular aggregative state effects can dominate surface dynamics.[15–20] It has been reported that for highly oriented surface chains, their diffusion rate perpendicular to the chain alignment direction is slower than that of the non-oriented chains.[16,17] Briggs *et al.*[18] found that a spherical self-entangled PS single chain on a film surface has a T_g lower than that of the equilibrated "melt-like" PS chains. Chang *et al.*[19] reported that the layer-by-layer aggregative structure of polymer chains prepared by the Langmuir–Blodgett technique gave rise to a thickness-independent T_g, while the T_g of the spin-coated

Department of Chemistry, Key Laboratory of Advanced Textile Materials and Manufacturing Technology of the Education Ministry, Zhejiang Sci-Tech University, Hangzhou 310018, China. E-mail: wxinping@yahoo.com; wxinping@zstu.edu.cn; Fax: +86-571-8684-3600; Tel: +86-571-8684-3600

† Electronic supplementary information (ESI) available: Size distribution of micelles of $PMMA_{430}$-ec-$PFMA_n$ in toluene, TEM images of $PMMA_{430}$-ec-$PFMA_n$ thin films, surface F/C ratio and water contact angle of $PMMA_{430}$-ec-$PFMA_n$ films, X-ray diffraction (XRD) profile of a $PMMA_{430}$-ec-$PFMA_{22}$ micelle film, XPS curves of a $PMMA_{430}$-ec-$PFMA_{22}$ micelle film annealed at various temperatures, time evolution of contact angle of a $PMMA_{430}$-ec-$PFMA_{22}$ film annealed at various temperatures and E_a determination for surface dynamics of $PMMA_{430}$-ec-$PFMA_n$ (n = 4–22) films. See DOI: 10.1039/c3sm50237f

films decreased with a reduction in film thickness. Fukuda *et al.*[15] demonstrated that the T_g of PMMA films can be enhanced by as much as ~30 °C compared to that of the spin-coated film, by end grafting the PMMA chain onto a silicon substrate. Recently, Tsui *et al.*[20] showed that only a slight reduction of the size of macromolecular coils in solution effectively slowed down the surface dynamics of the resultant film. Accordingly, it is apparent that the aggregative structures of chains play an important role on the resultant surface chain dynamics.

By spin coating kinetically frozen micelles from solution onto a substrate, a micellar film composed of densely packed dry micelles can be formed.[21–23] Unlike the "melt-like" structure of homopolymer chains in the condensed state, polymer chains in micelles films have a distinct "core–corona" anisotropic aggregative structure, with the corona-forming block tethered by a dense packed micelle core. Knowledge of the surface dynamics of the micellar films is of importance for determining the temperatures and time scales over which polymer-based dry micelles might attain their original morphologies upon annealing, and this is pivotal for the application of micelle-based nanomaterials.[24–28] More important is that the micelle films present an interesting opportunity for expanding the range of our studies of the surface dynamics of polymer chains with more versatile condensed structures and confining geometries. Therefore, a significant concern is raised about how and to what extent the "micelle-like" aggregative structure affects the surface dynamics of polymer chains. This is highly significant both in terms of an improved understanding of the surface dynamics at the molecular level and in the practical application of nanomaterials where stability is central to design issues.

Measurements of micelle corona glass transitions on film surfaces are challenging, given the nanoscale volumes and small volume fractions being probed. The current study is made possible by the first use of a fluorine-end labeling technique to determine surface dynamics in the PMMA corona of micelles films. In this paper, five different fluorinated PMMA surfaces with chain aggregative structures ranging from the randomly free chains to the micellized ones are fabricated by spin coating fluorinated end capped PMMA micelle solutions with various lengths of the end segments onto a substrate. The chain dynamics of non-micellized PMMA and micellized PMMA corona on film surfaces are accessed by detecting the temperature and time dependence of chain rearrangement through contact angle measurements. The effects of "micellar-like" chain aggregative structures on their surface dynamics are studied by comparing the onset temperature of rearrangement (T_R^{onset}) and the E_a of these films.

2 Experimental section

2.1 Materials

Poly(methyl methacrylate) polymers end-capped with various numbers of 2-perfluorooctylethyl methacrylate (FMA) units ($PMMA_{430}$-ec-$PFMA_n$) were synthesized in our lab using atom transfer radical polymerization (ATRP), as described in our previous works.[29,30] The chemical structure of the end-capped PMMA is shown in Fig. 1, and the detailed characteristics of the various fluorinated PMMAs are shown in Table 1. 2-Perfluorooctylethyl methacrylate was purchased from Sigma-Aldrich Inc.

2.2 Film formation

$PMMA_{430}$-ec-$PFMA_n$ was dissolved in toluene at a 2.0 wt% concentration and the polymer solution was filtered through a porous PTFE film. The polymer films were prepared by spin coating the $PMMA_{430}$-ec-$PFMA_n$ solution onto a fused silica substrate. The detailed procedure and the underlying physics of the spin-coating method can be found in ref. 31 and 32. The as-cast films were placed in a vacuum oven (50 °C) for 48 h to remove the residual solvents, then subjected to a subsequent annealing process in air for various times and temperatures for elucidating the surface dynamics. The thickness of the resulting films, evaluated by ellipsometry (M-50, JASCO Co., Ltd.), was around 120 nm (more than 20 times the radius of gyration (R_g) of the utilized PMMA), which was sufficient to avoid substrate and ultrathinning effects on the surface dynamics.[33,34]

2.3 Characterization

Variations in surface structure of the polymer films after annealing treatment in air were evaluated by contact angle measurement as previously reported.[35] Contact angles (θ) of water were measured by the sessile drop method at room temperature and ambient humidity with a Krüss (Hamburg, Germany) DSA-10 contact angle goniometer. Samples which had been heated in air were slowly cooled to room temperature before θ measurement. The volume of the water drops used in the measurements was always 5 μL. The reported θ values are the averages of at least eight different measurements taken within 10 seconds of applying each drop of water. In order to ensure that the results were sufficiently credible, the experimental errors in measuring the θ values were evaluated to be less than $\pm 2^\circ$.

X-ray photoelectron spectroscopy (XPS) was performed using a PHI5000C ESCA System with an Mg Kα X-ray source (1253.6 eV). The X-ray gun was operated at a power of 250 W and the high voltage was maintained at 140 KV. Spectra were acquired at a photoelectron emission angle of 15° ($\theta = 15^\circ$, sampling depth about 2.3 nm). The chamber pressure during analysis was approximately 1×10^{-8} Torr. All spectra were calibrated by the C_{1s} peak of the C–C bond at 284.6 eV.

The morphology of the top surfaces of the samples was investigated using an XEI-100 scanning probe microscope (SPM, PSIA Co.). SPM measurements were performed in air with

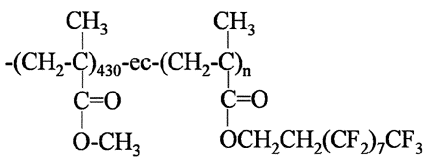

Fig. 1 Chemical structure of $PMMA_{430}$-ec-$PFMA_n$.

Table 1 Characteristics of $PMMA_{430}$-ec-$PFMA_n$ polymers synthesized by ATRP and the size of the micelles formed in toluene

Samples	$M_n \times 10^{-3}$	M_w/M_n [a]	W_F [c] (%)	n [d]	Micelle diameter [e] (nm)
$PMMA_{430}$-Br	43.0 [a]	1.12	—	—	—
$PMMA_{430}$-ec-$PFMA_2$	44.1 [b]	1.29	1.43	1.95	265
$PMMA_{430}$-ec-$PFMA_4$	45.3 [b]	1.29	3.00	4.2	255
$PMMA_{430}$-ec-$PFMA_7$	46.9 [b]	1.28	5.03	7.3	190
$PMMA_{430}$-ec-$PFMA_{12}$	49.5 [b]	1.17	8.02	12.3	132
$PMMA_{430}$-ec-$PFMA_{22}$	54.9 [b]	1.30	13.17	22.4	115

[a] Determined by GPC and calibrated by polystyrene standards. [b] Calculated from $PMMA_{430}$-ec-$PFMA_n$. [c] Fluorine content in polymers obtained by fluorine elemental analysis. [d] The number of FMA units (n) calculated by both fluorine content in the polymer and GPC results. Detailed calculation is described in the ESI.† [e] Hydrodynamic diameter of micelles in toluene obtained by dynamic light scattering (DLS).

an etched silicon probe having a length of 125 μm; the spring constant was varied from 20 to 75 N m^{-1}. Scanning was carried out in tapping mode at a frequency of approximately 300 Hz. Proton nuclear magnetic resonance spectroscopy (^{1}H NMR) spectra of $PMMA_{430}$-ec-$PFMA_n$ were recorded on a Bruker Avance AMX-400 NMR spectrometer in d_8-toluene with tetramethylsilane (TMS) as the internal standard.

The hydrodynamic diameters of the copolymers in a toluene solution were measured by dynamic light scattering with a 90 Plus NanoParticle Size Distribution Analyser (Brookhaven Instruments Ltd., UK). The polymer solutions were prepared at a concentration of 0.01 g mL^{-1} and were filtered through a 0.45 μm PTFE membrane.

3 Results and discussion

3.1 Fabrication of film surfaces with various chain aggregative structures

Toluene preferentially dissolves the PMMA block in $PMMA_{430}$-ec-$PFMA_n$, whereas the PFMA is almost insoluble.[36,37] As a consequence, the copolymers associate to form micelles in toluene and the micellization kinetics can be tuned by varying the polymerization degree of the solvophobic PFMA segments from 2 to 22, according to micelle kinetic theory of block copolymers.[38] Fig. S1 (ESI†) shows the distributions of the hydrodynamic diameters (D_h) of $PMMA_{430}$-ec-$PFMA_n$ micelles formed in toluene. The averaged D_h of the micelles decreases from ~260 to ~120 nm when the polymerization degree (n) of PFMA increases from 2 to 22, as shown in Fig. 2. Meanwhile, the size distribution of the micelles narrows with an increasing length of the PFMA block.

The influence of the length of the solvophobic PFMA block (n = 2–22) on the micellization kinetics of $PMMA_{430}$-ec-$PFMA_n$ in toluene was studied by ^{1}H NMR. Fig. 3 shows the ^{1}H NMR spectra of $PMMA_{430}$-ec-$PFMA_n$ in d_8-toluene at a concentration of 0.015 g mL^{-1}, and the spectrum of $PMMA_{430}$-ec-$PFMA_{22}$ with concentrations below its critical micelle concentration (CMC). The resonant peak at 3.72 ppm is attributed to the proton of the –O–CH_2 group in the FMA units.[39,40] It is evident in Fig. 3 that the peak at 3.72 ppm is gradually split into three adjacent peaks together with a broadening and downfield shifting (toward higher δ) by increasing the number of FMA units from 4 to 12. It was reported that the micellization kinetics of polymers can be quantified by the line-width of the NMR peak, since reduction in the mobility of the solvophobic block in a micelle core results in a broadening of the peak line-width of protons from the corresponding components.[41–44] It is reasonable to attribute the downfield shifting and broadening of the –O–CH_2 peak in the PFMA block to the change in the environment surrounding: the protons from toluene to fluorinated micelle core. In this case, the broadening of the line-width ($\Delta\upsilon$) of the –O–CH_2 peak with increasing PFMA block length can be attributed to a reduction in the mobility of the PFMA segments due to the core becoming increasingly compact. This was also confirmed by the ^{1}H NMR of $PMMA_{430}$-ec-$PFMA_{22}$ at a concentration lower than its CMC, as shown in Fig. 3. It is obvious that the broadening and shifting of the –O–CH_2 peak does not take place at this concentration for the non-micellized fluorinated PMMA unimers.

The line-width ($\Delta\upsilon$) of the –O–CH_2 peak in ^{1}H NMR was plotted against the number (n) of FMA units in $PMMA_{430}$-ec-$PFMA_n$ as shown in Fig. 2. It is clear that the ^{1}H NMR line-width of the –O–CH_2 peak in the FMA unit is about 48 Hz when the solvophobic PFMA block is short (n = 2, 4), which is the same as that of the $PMMA_{430}$-ec-$PFMA_{22}$ unimer below CMC. Overall,

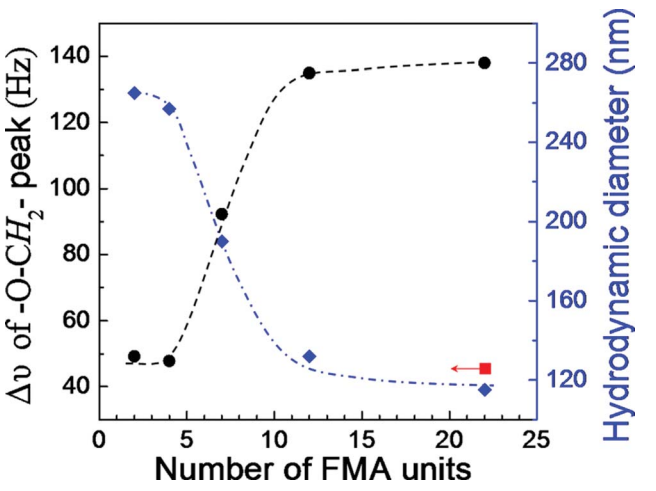

Fig. 2 ^{1}H NMR line-width ($\Delta\upsilon$) of the –O–CH_2 peak in FMA unit and the hydrodynamic diameters of the aggregates in solution as a function of the number of FMA units (n) in $PMMA_{430}$-ec-$PFMA_n$. Red square marker: the line-width of the –O–CH_2 peak for $PMMA_{430}$-ec-$PFMA_{22}$ at a concentration below its CMC.

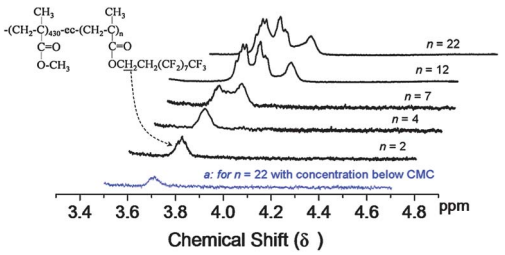

Fig. 3 ^{1}H NMR spectra of the –O–CH_2 peak of $PMMA_{430}$-ec-$PFMA_n$ (n = 2–22) in a d_8-toluene solution (0.015 g mL^{-1}). (a): ^{1}H NMR of a $PMMA_{430}$-ec-$PFMA_{22}$ solution with a concentration (0.00015 g mL^{-1}) below its CMC (0.00042 g mL^{-1}).

Fig. 2 and Fig. S1 (ESI†) show that these fluorinated PMMAs associate only to form very loose aggregates with larger diameters and broad size distributions. With an increase of n in $PMMA_{430}$-ec-$PFMA_n$, from 4 to 12, the formed micelles show a dramatic reduction in size and a sharp depression of chain kinetics, resulting in a considerable increase of $\Delta\upsilon$. This phenomenon suggests that kinetically frozen micelles start to form at $n = 7$ and the chain exchange rate slows down. When n = 12 and 22 in $PMMA_{430}$-ec-$PFMA_n$, frozen micelles are formed with similar diameters of around 120 nm and a narrow size distribution. Thus, the chain kinetics and micelle size do not vary significantly, resulting in an increase of $\Delta\upsilon$ up to 140 Hz. This behavior is the same as noted in previous reports that showed that as the length of the solvophobic block increased, the micelles formed more readily and became more stable.[38,45,46] Therefore, the results above indicate that a kinetically tunable micelle with a PMMA corona and a PFMA core was prepared by adjusting the length of the solvophobic PFMA segment in $PMMA_{430}$-ec-$PFMA_n$.

Polymer films with tunable macromolecular aggregative structures such as micelles can be prepared by spin coating micelle solutions with various micellization kinetics onto a substrate.[47] Fig. 4 shows the AFM topographic images of $PMMA_{430}$-ec-$PFMA_n$ spin-coated film surfaces. The AFM images exhibit very smooth surfaces with a RMS (root mean squared) roughness below 1.0 nm when the number (n) of FMA units is 2 and 4 in $PMMA_{430}$-ec-$PFMA_n$, which indicates that no preferred aggregation structures were formed on the fluorinated PMMA film surfaces. However, AFM images show the presence of "micelle-like" spherical domains on the film surfaces when n in $PMMA_{430}$-ec-$PFMA_n$ is above 7. These aggregations are due to the direct transfer of micelles from solution to the condensed film. Since the micellization kinetics of $PMMA_{430}$-ec-$PFMA_7$ in toluene are between those of the free chains and the completely frozen chains, the $PMMA_{430}$-ec-$PFMA_7$ micelle film is accordingly dominated by looser micelles (larger domain size) scattered on the surface (Fig. 4). When n is increased to 12 or 22, dense-packed spherical micelles are formed on the film surface. These aggregative structures of fluorinated PMMA films were further confirmed by TEM, as shown in Fig. S2 (ESI†).

The surface chemical compositions and properties of the spin-coated $PMMA_{430}$-ec-$PFMA_n$ films were characterized by X-ray photoelectron spectroscopy (XPS) and contact angle measurements. It can be observed from Fig. S3 (ESI†) that the water contact angles of fluorinated PMMA micelle films with 12 and 22 FMA units are very close to that of the PMMA homopolymer, indicating that these film surfaces were covered by the PMMA segment without PFMA enrichment. This was also evidenced by XPS analysis, in which the F/C ratios of $PMMA_{430}$-ec-$PFMA_{12}$ and $PMMA_{430}$-ec-FMA_{22} film surfaces are close to zero. The extremely low fluorine contents on the $PMMA_{430}$-ec-$PFMA_{12}$ and $PMMA_{430}$-ec-FMA_{22} film surfaces are indicative of the presence of "micelle-like" aggregative structures, with corona-forming PMMA chains covering the outermost surface and PFMA buried in the micelle core, as shown in Scheme 1.

Both $PMMA_{430}$-ec-$PFMA_2$ and $PMMA_{430}$-ec-$PFMA_4$ could not form stable micelles in toluene. During the film formation process, the loose aggregates disassembled resulting in a random distribution of the fluorinated chains at the surface as shown in Scheme 1. The results above suggest that two different types of films, either micellized PMMA tethered by a PFMA micelle core or non-micellized free PMMA chains, are fabricated by spin coating a solution of PMMA end-capped with various numbers of FMA units onto silica substrates.

3.2 Surface glass transition behavior of PMMA chains constrained by a micelle core

With the annealing of $PMMA_{430}$-ec-$PFMA_n$ films, reorganization at the film surface occurred to attain an equilibrium surface structure with minimal surface energy. The contact angle measurement is an effective method to detect the surface rearrangement of the fluorinated PMMA films by tracing the enrichment of PFMA on the film surface. Fig. 5 shows the water contact angles of non-micellized $PMMA_{430}$-ec-$PFMA_2$ and $PMMA_{430}$-ec-$PFMA_4$ film surfaces as function of the annealing temperature. Two plateaus in the temperature *vs.* contact angle curve are found for these samples. The first plateau at low temperatures demonstrates a temperature independent contact angle, which corresponds to the glassy surface. After this plateau, a large increase of the contact angle occurs with increasing temperature. As the temperature reaches above ~110 °C, the chains' mobility was extremely high due to the close bulk T_g of PMMA. The surface chains are able to attain its equilibrated structure during annealing, which resulted in the contact angle attaining its corresponding saturated value. A least-squares linear fitting of the straight line was used to approximate the temperature dependence of the structural relaxation of the surface chains. The onset temperature for the surface chain rearrangement (T_R^{onset}) is determined by the temperature at the intersection point of the two straight lines at which the first discontinuity occurs (shown in Fig. 5). The result shows that these two non-micellized fluorinated PMMA films share the same T_R^{onset} of 70 °C.

Next, we focus on the T_R^{onset} measurement of the micellized PMMA with 7, 12 and 22 FMA units. As evident from the above results, the fluorinated PMMA with 7, 12 and 22 FMA units associated as micelles on the film surfaces, with a PFMA core buried inside the PMMA corona (Scheme 1). Fig. 5 illustrates the change of water contact angle of micellized fluorinated PMMA

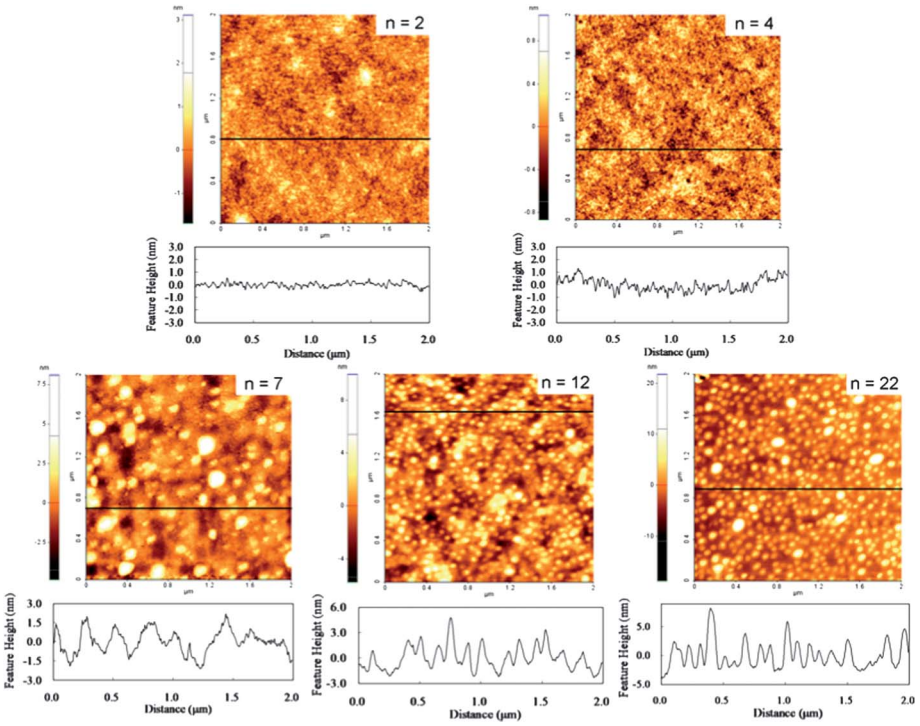

Fig. 4 AFM topographic images of $PMMA_{430}$-ec-$PFMA_n$ film surfaces.

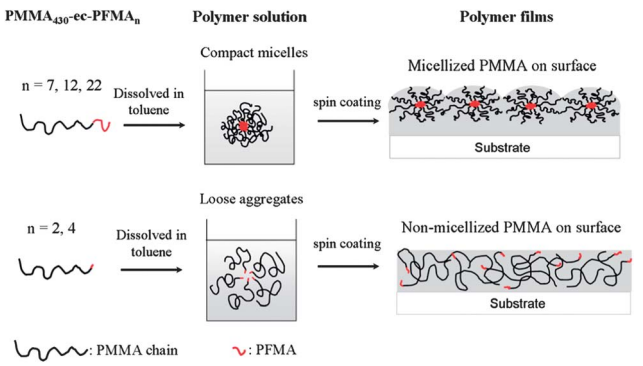

Scheme 1 Schematic of the fabrication of non-micellized (bottom) and micellized (top) PMMA chains on film surfaces.

($n = 7$, 12, 22) as a function of the annealing temperature. The T_R^{onset} of the micellized PMMA with 7, 12 and 22 FMA units was determined to be 78 °C, 82 °C and 83 °C, respectively. The onset temperature of the chain rearrangement T_R^{onset} for $PMMA_{430}$-ec-$PFMA_n$ film surfaces as a function of the length (n) of the solvophobic PFMA segment is plotted in Fig. 6. The results show that T_R^{onset} is 70 °C and does not change with the number of FMA units (n) when this value is below 5. T_R^{onset} increases sharply to 82 °C when the number of FMA units (n) increased from 5 to 12 and remains at the almost constant value of 83 °C when n was up to 22.

The surface roughness analysis of fluorinated PMMA films before and after annealing by AFM demonstrates that the effect of physical roughness on contact angle is negligible. Therefore, the variation in contact angles shown above was solely associated with the surface chemical structures of the films, due to surface chain rearrangement. The chemical composition of the topmost surface region was quantitatively analyzed by XPS. Fig. 7 shows the F/C ratios for $PMMA_{430}$-ec-$PFMA_2$ films after being annealed at various temperatures. As evident in Fig. 7, the onset temperature for surface F/C ratio incrementation is 70.5 °C. The XPS result correlates well with the contact angle measurements and confirm that the increment of water contact angle for the fluorinated PMMA films after being annealed is due to the segregation of the end-capped fluorinated components.

AFM was employed to trace the morphology evolution of the surface micelles on a $PMMA_{430}$-ec-$PFMA_{22}$ film surface under annealing, as shown in Fig. 8. When the annealing temperature is below 76 °C, the morphology of the surface micelles is unchanged and does not show any apparent collapse or break up. By increasing the temperature to 85 °C, small pores are observed on the apex of the micelles, which means that the glassy PMMA is starting to rubberize and the PFMA segments underneath the PMMA corona diffuse to the surface. This was also confirmed by the surface fluorine content analysis. Fig. S4 (ESI†) shows that the PFMA inside the micelles core starts to enrich when the annealing temperature reaches above ~85 °C. These evidence verifies that the enrichment of PFMA and the opening of the PMMA shell of the micelles are two cooperative and coupled processes. By further increasing the annealing temperature to 97 °C, the pore progressively develops into cavitations with diameters of approximately 80 nm and depths

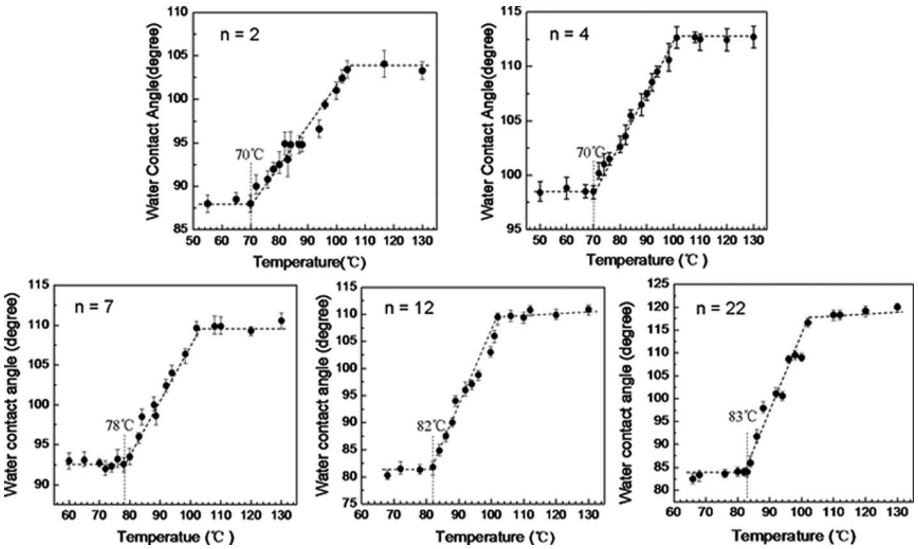

Fig. 5 Water contact angle of spin-coated $PMMA_{430}$-ec-$PFMA_n$ (n = 2–22) films as a function of annealing temperature. Annealing time: 24 h.

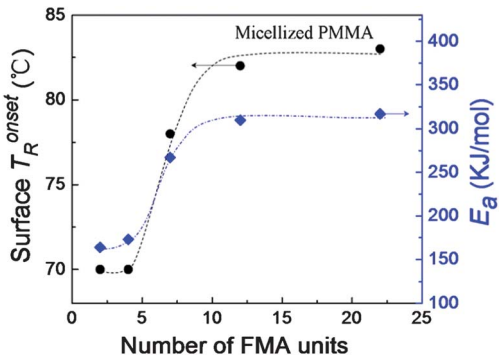

Fig. 6 Onset temperature of chain rearrangement T_R^{onset} and the energy barrier (E_a) for the relaxation for $PMMA_{430}$-ec-$PFMA_n$ film surfaces with different numbers of FMA units.

near 6.5 nm. The formation of cavitations is thermodynamically driven by the migration of PFMA towards the surface, and kinetically controlled by the mobility of the PMMA chains. Notably, the onset temperature of the chain rearrangement T_R^{onset} (83 °C) of micellized PMMA with 22 FMA units is close to the onset temperature of ~85 °C for the PMMA corona opening. Additionally, the film surface dominated by micelles or cavitations has a RMS roughness in the range of 2 to 5 nm, which is well below the lower limits of the surface roughness of 100 nm necessary to affect wettability.[48] Thus, it is believed that the surface morphology change from micelles to cavitations does not affect the contact angle.

To attain a minimum surface free energy, the PFMA segments buried inside the PMMA film would diffuse outwards to cover the film surface. The surface reorganization can be attained in the annealing temperature range at which PMMA or PFMA segments can change their aggregation state on a large scale, that is, when their micro-Brownian motions start. Since PFMA has a T_g near room temperature,[49] and X-ray diffraction (XRD) illustrates an amorphous PFMA core (Fig. S5, ESI†), the migration of PFMA to the film surface is kinetically controlled by the mobility of the PMMA corona. In addition, it was verified that the difference in transporting time for FMA diffusing from the micelle cores to the film surface does not affect the

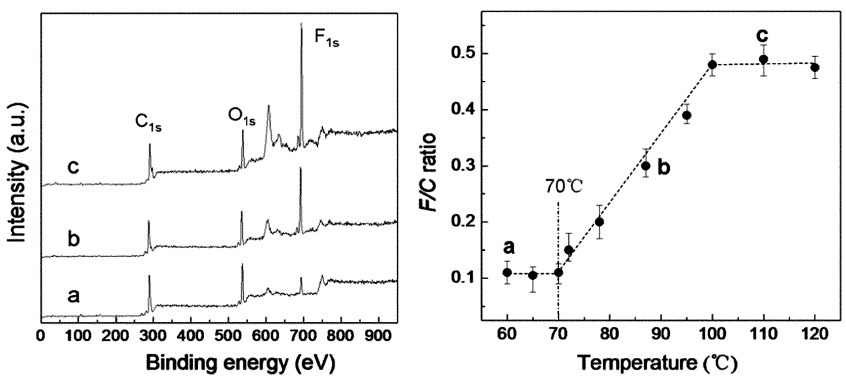

Fig. 7 XPS spectra (left) and F/C ratios (right) of $PMMA_{430}$-ec-$PFMA_2$ spin-coated films as a function of the annealing temperature (24 h). The letters a, b and c in the left graph assigned to the XPS curve correspond to the sample with the selected annealing temperature as presented in right graph. The photoelectron emission angle (θ) was 15°.

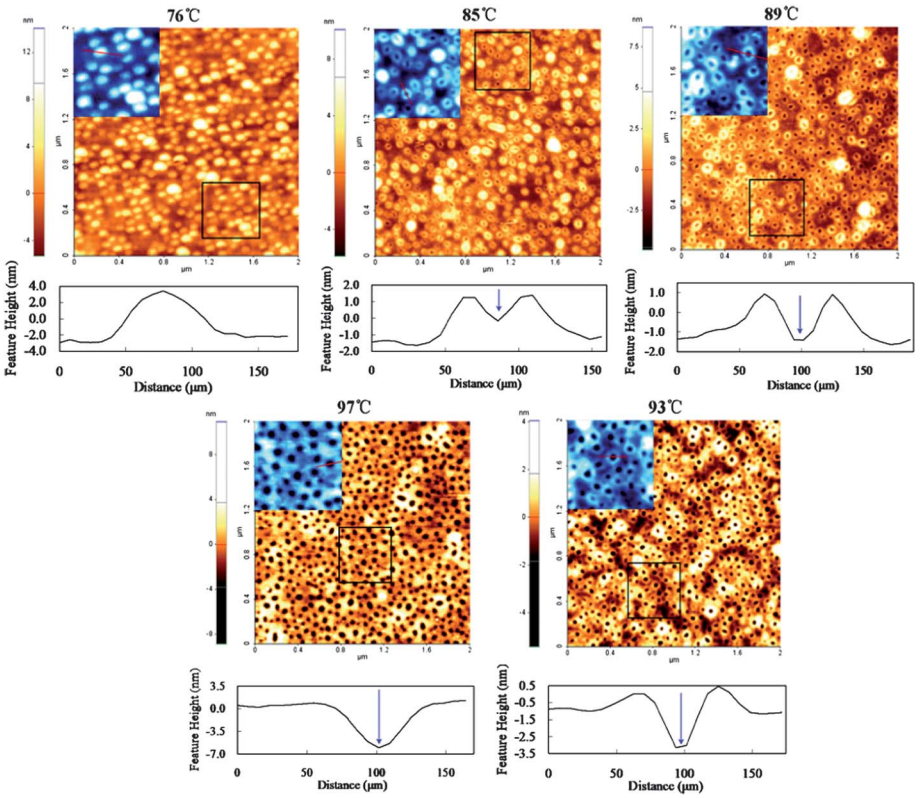

Fig. 8 Evolution of the surface morphology of $PMMA_{430}$-ec-$PFMA_{22}$ films as function of the annealing temperature (24 h) by AFM. Inset: magnifications of the boxed area (500 × 500 nm). Below: cross-sectional profiles along the red line in the corresponding inset image, describing the opening process of a single surface micelle. The arrowheads indicate the pore.

measured T_R^{onset}, as illustrated in Section 7 in the ESI.† Therefore, the currently observed T_R^{onset} has its physical meaning in terms of the onset temperature for the frozen PMMA transferred into a mobile state on a laboratory time scale. Therefore, the onset temperature of rearrangement (T_R^{onset}) of a fluorinated PMMA surface should be related to the surface T_g of PMMA chains. The result shows that the two non-micellized PMMA film surfaces with 2 and 4 FMA units share the same T_R^{onset} of 70 °C, which is close to the surface relaxation temperature of PMMA (67 °C) measured by polarization-rotating sum frequency generation vibrational spectroscopy.[50]

3.3 Effect of chain aggregative structure on the surface dynamics of PMMA chains

Contact angle measurement is one of the most sensitive methods for studying surface reconstruction and chain relaxation.[33,51–53] The apparent activation energy (E_a) for the surface relaxation of fluorinated PMMA films with various aggregative structures was examined on the basis of the time-temperature superposition principle for chain dynamics. Water contact angle measurements of the films was employed to evaluate their surface relaxation. Fig. 9 displays the time dependence of the measured contact angle for a $PMMA_{430}$-ec-$PFMA_2$ film at different temperatures. The water contact angles exhibit an exponential increment with increasing annealing time. The relaxation rate is highly dependent on the temperature: a higher temperature results in a shorter time to attain a meta-stable contact angle. We re-scaled the abscissa of each curve in Fig. 9 with a temperature-dependent shift factor, α_T, using 85 °C as the reference temperature (T_s), to qualitatively describe the time and temperature dependence of the surface relaxation (a vertical shift is also conducted). The curves in Fig. 9a are super-imposed onto a master curve shown in Fig. 9b. This clearly demonstrates that a time-temperature equivalence property, which is characteristic of the bulk viscoelastic properties of polymeric materials, can be also applied to the surface relaxation of the PMMA film.

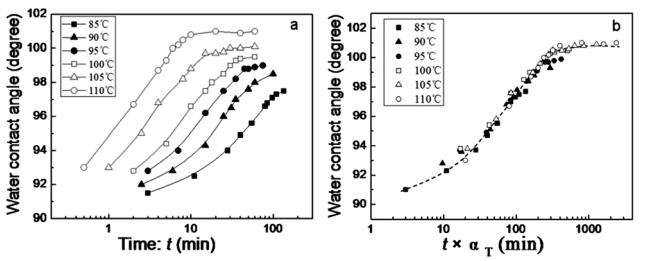

Fig. 9 (a) Time evolution of the water contact angle of a $PMMA_{430}$-ec-$PFMA_2$ film annealed at various temperatures. (b) Master curve of the annealing time-contact angle relationship for $PMMA_{430}$-ec-$PFMA_2$ films drawn from each curve in (a) with the abscissa re-scaled by a temperature-dependent shift factor, α_T, (reference temperature (T_s): 85 °C). The dashed line in panel (b) is drawn to guide the eye.

Fig. 10 shows the relationship between α_T and the annealing temperature, which corresponds to a linear Arrhenius plot. The appearance of an Arrhenius-related linear superposition argues that the surface chains have a temperature-independent activation energy for relaxation, which is different from the WLF-like chain relaxation in bulk. Similar Arrhenius-related polymer surface dynamics have previously been observed in the literature.[9,51,53] The apparent activation energy for surface relaxation can be obtained by fitting the data in Fig. 10 with the modified Arrhenius equation described by the following:[54]

$$\log \alpha_T = -\frac{E_a}{2.303R}\left(\frac{1}{T}-\frac{1}{T_s}\right) \quad (1)$$

where R is the gas constant and E_a is the apparent activation energy for surface relaxation. The apparent activation energy (E_a) for surface relaxation of $PMMA_{430}$-ec-$PFMA_2$ is estimated from the slope in Fig. 10 to be 164 kJ mol^{-1}, which is lower than the E_a for the α relaxation of bulk PMMA (460 kJ mol^{-1}).[55] This lower activation energy for the film indicates that the mobility of the polymer chains on the film surface is substantially enhanced compared to that in the bulk, which is in accordance with the results deduced by scanning probe microscopy.[56,57]

The E_a of PMMA with various surface aggregative structures of $PMMA_{430}$-ec-$PFMA_n$ (n = 4–22) films are determined by the same time-temperature equivalent shift of the contact angle *vs.* the annealing time curves, and the linear correlations between the logarithmic α_T and $1/T - 1/T_s$ are shown in Fig. S7 (ESI†). The E_a data for the surface dynamics of PMMA in $PMMA_{430}$-ec-$PFMA_n$ with various FMA units sre presented in Fig. 6. The E_a for the surface dynamics of the non-micellized PMMA chains with $n = 2$ and 4 are very similar, with the E_a values of 164 and 173 kJ mol^{-1}, respectively. For the micellized PMMA chains with 7, 12 and 22 FMA units, E_a is measured to be 267 kJ mol^{-1}, 310 kJ mol^{-1} and 317 kJ mol^{-1}, respectively. The E_a for the micellized PMMA on the surface is about twice as high as that of the non-micellized chains. Thus, it can be predicted from the magnitude of the activation energy that the energy barrier of thermal molecular motion for the micellized chains may be increased in comparison with that for the non-micellized free chains.

Fig. 11 shows that the onset temperature of chain rearrangement T_R^{onset} and its corresponding energy barrier (E_a) for $PMMA_{430}$-ec-$PFMA_n$ film surfaces as a function of the ^{1}H NMR line-width ($\Delta\upsilon$) of the –O–CH_2 peak in the PFMA block in solution. The results show that both T_R^{onset} and E_a increase linearly with an increasing $\Delta\upsilon$ of the corresponding solution with the slope of 0.14 and 1.65, respectively. These observations suggest that a more compact PFMA core of fluorinated polymer micelles in the casting solution results in slower surface dynamics of the corresponding spin-coated film. The slopes of the T_R^{onset} and E_a *vs.* $\Delta\upsilon$ correlations should indicate how greatly the surface dynamics of solid films was affected by the chains aggregative structure in solution. For $PMMA_{430}$-ec-$PFMA_{12}$ and $PMMA_{430}$-ec-$PFMA_{22}$ micelle films, the dense-packed micelle core serves as an "anchoring point" to interlink the corona-forming PMMA chains together, whose structure is analogous to polymer chains grafted onto a nanoparticle surface.

Next, based on the "micelle-like" aggregative structure, we propose speculative hypotheses for rationalizing the observed slower surface dynamics of the PMMA tethered by a micellar core. Adam–Gibbs theory suggests that the reduction of the configurational entropy could induce an increment of relaxation time, thus enhancing T_g.[58–60] The reduction of conformational freedom of the micellized chains is an interpretation of the lowered dynamics of the surface PMMA constrained in the micelle core. Since the chain connectivity of PMMA by the PFMA core imposes certain limitations on the molecular degrees of freedom, more energy is needed for the PMMA segments to move, thereby restricting the segment mobility and increasing T_g. Such a constraints effect on chain mobility is vividly illustrated by the slowing down of the chain dynamics upon tethering of the polymer chains onto a spherical nano-particle surface.[61–64] Matyjaszewski *et al.*[62] found that the T_g of poly(styrene) chains grafted onto a silica nano-particle surface was 13 K higher than that of the ungrafted free chains.

Alternatively, the chain ends are necessarily associated with a greater free volume and lower T_g. Mayes[65] and Kajiyama *et al.*[66,67]

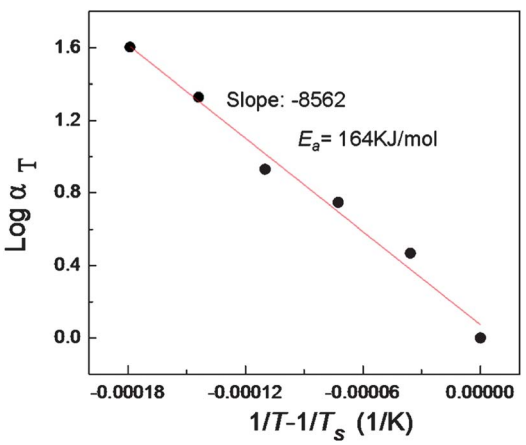

Fig. 10 Arrhenius plots of α_T *vs.* temperature for $PMMA_{430}$-ec-$PFMA_2$ films. The solid line is a linear least-square fit to the data from eqn (1) with a slope for elucidating the activation energy.

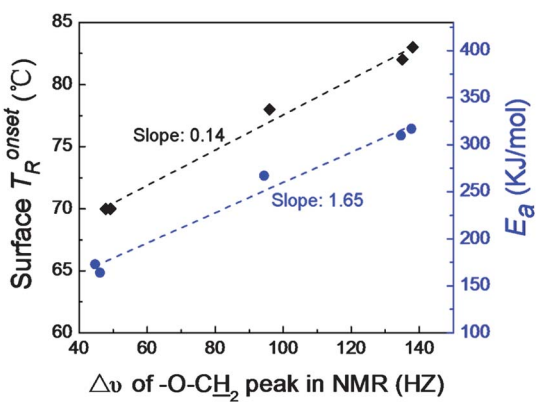

Fig. 11 Relationship between the ^{1}H NMR line-width ($\Delta\upsilon$) of the –O–CH_2 peak in PFMA block in solution and the surface dynamics (T_R^{onset} and E_a) of the resulting spin-coated film. The slopes of the fitted lines are indicated in the figure.

have shown that the localization of the chain ends on film surfaces increases the excess free volume, therefore substantially suppressing T_g and enhancing the mobility of the surface chains. For the micellized PMMA, the PMMA chains are interlinked together by the PFMA core, which halves the number of end groups per PMMA chain. Meanwhile, the tethering of PFMA in a micelle core hinders the enrichment of chain ends toward the film surface. These effects effectively reduce the pore volume available for chain motion on the surface, thus slowing down the rotation and translation of PMMA segments. Finally, a more tentative explanation is proposed based on the considerations related to the increase of chain packing density upon constraining PMMA in the micelles. The PMMA chain tethered by the micelle core is more able to adopt an anisotropic stretched conformation, rather than the random-coil conformation of non-micellized chains. The surface micelles of $PMMA_{430}$-ec-$PFMA_{22}$ have a radius (~55 nm, Fig. 4) very close in size to the length of a stretched $PMMA_{430}$ chain (~56 nm), which suggests a stretched conformation for the micellized PMMA chains. This anisotropic chain conformation facilitates the dense-packing of the PMMA chains. Fukuda *et al.* demonstrated that the T_g of PMMA chains grafted on a planar substrate is several tens of Kelvin degrees higher than that of the spin-coated films, due to the high packing density of the stretched chains grafted on the substrate.[15,68] Therefore, in our case, the micellized PMMA chain may adopt a close-packed stretching conformation, which would accordingly reduce the chain dynamics.

4 Conclusion

In summary, we present an experimental investigation of the surface dynamics of PMMA adopting various aggregative structures from the non-micellized free chains to the micellized chains tethered by a fluorinated block core. By tracing the reorganization of the chains on the surface, it is shown that the chain aggregative structures significantly influence the surface dynamics of PMMA. The results indicate that the relaxation activation energy (E_a) and the onset temperature of surface rearrangement (T_R^{onset}) of the micellized PMMA are much higher than those of the non-micellized free chains. This T_R^{onset} should be related to the surface glass temperature of PMMA. The enhanced surface T_R^{onset} and higher E_a for the micellized PMMA suggest that the tethering of PMMA chains to a micelle core substantially reduces their chain dynamics on the surface. The surface dynamics of PMMA are well correlated to the compactness of the PFMA core: a more compact PFMA core results in decrease of PMMA segment mobility on the surface. This slowed surface dynamics of the PMMA chains with "micellar-like" aggregative structure is rationalized by invoking three possible explanations, the reduction of free volume, the constraining of the conformational freedom and the increase of chain packing density. This study demonstrates the idea that the surface aggregative structure is a crucial factor affecting the chain dynamics on a film surface and a "core–corona" aggregative structure effectively suppresses the chain dynamics of a corona-forming block on the surface, which may be a potential pathway to increasing the thermal stability of nanomaterials.

Acknowledgements

We are thankful for support from the National Natural Science Foundation of China (NSFC, no. 21174134) and the Natural Science Foundation of Zhejiang Province (Grant no. Z4100463).

References

1 R. A. L. Jones and R. W. Richard, *Polymers at Surfaces and Interfaces*, Cambridge University Press, Cambridge, 1999.
2 B. Zuo, F. F. Zheng, Y. R. Zhao, T. Y. Chen, Z. H. Yan, H. Ni and X. P. Wang, *Langmuir*, 2012, **28**, 4283–4292.
3 C. R. Daley, Z. Fakhraai, M. D. Ediger and J. A. Forrest, *Soft Matter*, 2012, **8**, 2206–2212.
4 C. Kim, A. Facchetti and T. J. Marks, *Science*, 2007, **318**, 76–80.
5 B. Zuo, C. Qian, D. Yan, Y. Liu, W. Liu, H. Fan, H. Tian and X. P. Wang, *Macromolecules*, 2013, **46**, 1875–1882.
6 H. G. Peng, Y. P. Kong and A. F. Yee, *Macromolecules*, 2010, **43**, 409–417.
7 Z. Fakhraai and J. A. Forrest, *Science*, 2008, **319**, 600–604.
8 C. J. Ellison and J. M. Torkelson, *Nat. Mater.*, 2003, **2**, 695–700.
9 Z. Yang, Y. Fujii, F. K. Lee, C. H. Lam and O. K. C. Tsui, *Science*, 2010, **328**, 1676–1679.
10 R. D. Priestley, C. J. Ellison, L. J. Broadbelt and J. M. Torkelson, *Science*, 2005, **309**, 456–459.
11 R. D. Priestley, *Soft Matter*, 2009, **5**, 919–926.
12 J. A. Forrest and K. Dalnoki-Veress, *Adv. Colloid Interface Sci.*, 2001, **94**, 167–196.
13 K. Tanaka, A. Takahara and T. Kajiyama, *Macromolecules*, 1998, **31**, 863–869.
14 J. L. Keddie, R. A. L. Jones and R. A. Cory, *Faraday Discuss.*, 1994, **98**, 219–230.
15 S. Yamamoto, Y. Tsujii and T. Fukuda, *Macromolecules*, 2002, **35**, 6077–6079.
16 Y. Pu, H. White, M. H. Rafailovich, J. Sokolov, S. A. Schwarz, A. Dhinojwala, D. M. G. Agra and S. Kumar, *Macromolecules*, 2001, **34**, 4972–4977.
17 A. D. Schwab, D. M. G. Agra, J. H. Kim, S. Kumar and A. Dhinojwala, *Macromolecules*, 2000, **33**, 4903–4909.
18 V. N. Bliznyuk, H. E. Assender and G. A. D. Briggs, *Macromolecules*, 2002, **35**, 6613–6622.
19 Y. K. See, J. Cha, T. Chang and M. Ree, *Langmuir*, 2000, **16**, 2351–2355.
20 R. N. Li, A. Clough, Z. Yang and O. K. C. Tsui, *Macromolecules*, 2012, **45**, 1085–1089.
21 Z. Chen, C. He, F. Li, L. Tong, X. Liao and Y. Wang, *Langmuir*, 2010, **26**, 8869–8874.
22 A. C. Miller, R. D. Bennett, P. T. Hammond, D. J. Irvine and R. E. Cohen, *Macromolecules*, 2008, **41**, 1739–1744.
23 B. H. Sohn, S. Yoo, B. W. Seo, S. H. Yun and S. M. Park, *J. Am. Chem. Soc.*, 2001, **123**, 12734–12735.
24 D. Quemener, G. Bonniol, T. N. T. Phan, D. Gigmes, D. Bertin and A. Deratani, *Macromolecules*, 2010, **43**, 5060–5065.
25 E. Q. Chen, Y. Xia, M. J. Graham, M. D. Foster, Y. Mi, W. L. Wu and S. Z. D. Cheng, *Chem. Mater.*, 2003, **15**, 2129–2135.

26 K. Albrecht, A. Mourran and M. Moeller, *Adv. Polym. Sci.*, 2006, **200**, 57–70.
27 P. Tyagi, A. Deratani, D. Bouyer, D. Cot, V. Gence, M. Barboiu, T. N. T. Phan, D. Bertin, D. Gigmers and D. Quemener, *Angew. Chem., Int. Ed.*, 2012, **51**, 7166–7170.
28 C. Y. Chang, P. J. Wu and Y. S. Sun, *Soft Matter*, 2011, **7**, 9140–9147.
29 H. Ni, X. H. Li, Y. Y. Hu, B. Zuo, Z. L. Zhao, J. P. Yang, D. X. Yuan, X. Y. Ye and X. P. Wang, *J. Phys. Chem. C*, 2012, **116**, 24151–24160.
30 X. F. Wang, H. Ni, D. W. Xue, X. P. Wang, R. Feng and H. F. Wang, *J. Colloid Interface Sci.*, 2008, **321**, 373–383.
31 K. Norrman, A. Ghanbari-Siahkali and N. B. Larsen, *Annu. Rep. Prog. Chem., Sect. C*, 2005, **101**, 174–201.
32 D. B. Hall, P. Underhill and J. M. Torkelson, *Polym. Eng. Sci.*, 1998, **38**, 2039–2045.
33 M. K. Mukhopadhyay, X. Jiao, L. B. Lurio, Z. Jiang, J. Stark, M. Sprung, S. Narayanan, A. R. Sandy and S. K. Sinha, *Phys. Rev. Lett.*, 2008, **101**, 115501.
34 X. P. Wang, X. Xiao and O. K. C. Tsui, *Macromolecules*, 2001, **34**, 4180–4185.
35 X. P. Wang, X. B. Wang and Z. F. Chen, *Polymer*, 2007, **48**, 522–529.
36 Y. Li, L. Meli, K. T. Lim, K. P. Johnston and P. F. Green, *Macromolecules*, 2006, **39**, 7044–7054.
37 Y. Urushihara and T. Nishino, *Langmuir*, 2005, **21**, 2614–2618.
38 T. Nicolai, O. Colombani and C. Chassenieux, *Soft Matter*, 2010, **6**, 3111–3118.
39 M. D. Dimitriou, Z. Zhou, H. S. Yoo, K. L. Killops, J. A. Finlay, G. Cone, H. S. Sundaram, N. A. Lynd, K. P. Barteau, L. M. Campos, D. A. Fischer, M. E. Callow, J. A. Callow, C. K. Ober, C. J. Hawker and E. J. Kramer, *Langmuir*, 2011, **27**, 13762–13772.
40 D. W. Xue, X. P. Wang, H. Ni, W. Zhang and G. Xue, *Langmuir*, 2009, **25**, 2248–2257.
41 Z. Gao, X. F. Zhong and A. Eisenberg, *Macromolecules*, 1994, **27**, 794–802.
42 T. Nivaggioli, B. Tsao, P. Alexandridis and T. A. Hatton, *Langmuir*, 1995, **11**, 119–126.
43 F. Petit-Agnely and I. Iliopoulos, *J. Phys. Chem. B*, 1999, **103**, 4803–4808.
44 N. Li, S. Zhang, L. Zheng, J. Wu, X. Li and L. Yu, *J. Phys. Chem. B*, 2008, **112**, 12453–12460.
45 K. Matsumoto, M. Kubota, H. Matsuoka and H. Yamaoka, *Macromolecules*, 1999, **32**, 7122–7127.
46 A. G. Denkova, E. Mendesb and M. O. Coppens, *Soft Matter*, 2010, **6**, 2351–2357.
47 R. D. Bennett, A. C. Miller, N. T. Kohen, P. T. Hammond, D. J. Irvine and R. E. Cohen, *Macromolecules*, 2005, **38**, 10728–10735.
48 H. J. Busscher, A. W. J. van Pelt, P. de Boer, H. P. de Jong and J. Arends, *Colloids Surf.*, 1984, **9**, 319–331.
49 K. Honda, M. Morita, O. Sakata, S. Sasaki and A. Takahara, *Macromolecules*, 2010, **43**, 454–460.
50 Q. Li, R. Hua, I. J. Cheah and K. C. Chou, *J. Phys. Chem. B*, 2008, **112**, 694–697.
51 A. Horinouchi, H. Atarashi, Y. Fujii and K. Tanaka, *Macromolecules*, 2012, **45**, 4638–4642.
52 Y. Wang, J. Sun and L. Li, *Langmuir*, 2012, **28**, 6151–6156.
53 D. Wong, C. A. Jalbert, P. A. O'Rourke-Muisener and J. T. Koberstein, *Macromolecules*, 2012, **45**, 7973–7984.
54 S. Kasapis and P. Shrinivas, *J. Agric. Food Chem.*, 2010, **58**, 3825–3832.
55 S. Saito and T. Nakajima, *J. Appl. Polym. Sci.*, 1959, **2**, 93–99.
56 K. Tanaka, A. Takahara and T. Kajiyama, *Macromolecules*, 2000, **33**, 7588–7593.
57 N. Satomi, K. Tanaka, A. Takahara, T. Kajiyama, T. Ishizone and S. Nakahama, *Macromolecules*, 2001, **34**, 8761–8767.
58 J. H. Gibbs and E. A. DiMarzio, *J. Chem. Phys.*, 1958, **28**, 373–383.
59 G. Adam and J. H. Gibbs, *J. Chem. Phys.*, 1965, **43**, 139–146.
60 K. L. Ngai, *J. Non-Cryst. Solids*, 2000, **275**, 7–51.
61 H. Oh and P. F. Green, *Nat. Mater.*, 2008, **8**, 139–143.
62 D. A. Savin, J. Pyun, G. D. Patterson, T. Kowalewski and K. Matyjaszewski, *J. Polym. Sci., Part B: Polym. Phys.*, 2002, **40**, 2667–2676.
63 L. Zhu, X. Wang, Q. Gu, W. Chen, P. Sun and Gi. Xue, *Macromolecules*, 2013, **46**, 2292–2297.
64 K. Hayashida, H. Tanaka and O. Watanabe, *Polym. Int.*, 2011, **60**, 1194–1200.
65 A. M. Mayes, *Macromolecules*, 1994, **27**, 3114–3115.
66 F. Xie, H. F. Zhang, F. K. Lee, B. Du, O. K. C. Tsui, Y. Yokoe, K. Tanaka, A. Takahara, T. Kajiyama and T. He, *Macromolecules*, 2002, **35**, 1491–1492.
67 T. Kajiyama, K. Tanaka and A. Takahara, *Macromolecules*, 1997, **30**, 280–285.
68 K. Urayama, S. Yamamoto, Y. Tsujii, T. Fukuda and D. Neher, *Macromolecules*, 2002, **35**, 9459–9465.